

Polyynes Electronic and Vibrational Properties under Environmental Interactions

M. Wanko,¹ Seymour Cahangirov,^{1,2} Lei Shi,³ Philip Rohringer,³ Zachary J. Lapin,⁴ Lukas Novotny,⁴ Paola Ayala,^{3,5} Thomas Pichler,³ and Angel Rubio^{1,6}

¹ Nano-Bio Spectroscopy Group and European Theoretical Spectroscopy Facility (ETSF), Universidad del País Vasco, CFM CSIC-UPV/EHU-MPC & DIPC, 20018 San Sebastián, Spain

² UNAM-National Nanotechnology Research Center, Bilkent University, 06800 Ankara, Turkey

³ University of Vienna, Faculty of Physics, 1090 Wien, Austria

⁴ ETH Zürich, Photonics Laboratory, 8093 Zürich, Switzerland

⁵ Yachay Tech University, School of Physical Sciences and Nanotechnology, 100119-Urcuquí Ecuador

⁶ Max Planck Institute for the Structure and Dynamics of Matter, Hamburg, Germany

(Dated: 01/04/2016)

Recent advances allow growing linear carbon chains of up to thousands of atoms inside carbon nanotubes [L. Shi et al., (in press), DOI: 10.1038/NMAT4617)]. This increases the interest in the unique properties of carbyne and finite polyynes and their response to different environments. Here, the experimental characterization still relies on empirical or bulk-physical models appropriate for specific chain lengths or environments. The physical understanding of the observed trends in terms of charge transfer, electron delocalization, and van-der-Waals interactions is widely missing. Here, we theoretically describe the main interactions between polyynes and graphene or carbon nanotubes to inspire future models that better account for experimental conditions.

Carbyne, an infinite sp^1 hybridized carbon chain, once controversially discussed as a mere hypothetical 1D allotrope, is today considered a promising candidate for new materials. Its theoretically predicted strength and elastic modulus are greater than that of any known material, including diamond, carbon nanotubes (CNTs) and graphene. Proposed applications include composite materials [1] and the smallest-possible field-effect transistor [2]. Advances in the synthesis of sp^1 -carbon oligomers of well-defined length and capped with bulky end groups have provided a detailed spectroscopic characterization of chains containing up to 22 triple bonds (number of chain atoms $N=44$) in solution [3]. A prominent feature, which polyynes share with polyenes, is an intense Raman band associated with the eigen mode of the longitudinal-optical (LO) branch of the conjugated polymer close to the Γ -point (called \mathcal{R} -mode in Zerbi's effective conjugation coordinate theory [4, 5]). The Γ -mode is a vibration of the bond-length alternation (BLA), where all triple bonds stretch in phase. Raman experiments [6] have revealed a nearly linear relation between N and the frequency of the Γ -mode (Fig. 1), which provides a convenient tool for length assignment of polyynes in solution, within this range. Resonant Raman spectroscopy has been used to detect polyynes inside carbon nanotubes [7–12], corroborated by high-resolution transmission electron microscopy (HRTEM). Here, the assignment of chain lengths is more difficult because chains with more than 16 atoms have been grown in tubes by annealing [13–15] and their exact length is unknown. Recently, we measured chain-band frequencies around 1800 cm^{-1} for individual polyynes of more than 1000 atoms encapsulated in DWCNTs using near-field optical Raman spectroscopy [16], where the length can be obtained directly from the near-field image (inset in Fig. 1). These frequencies show a variation of 17 cm^{-1} and are close to the linear extrapolation of the short-chain data to infinite N . Ab initio SCS-MP2 calculations [16], on the other hand, show

a saturation of the frequency softening for chains longer than $N=50$ atoms, inline with scaled and extrapolated B3LYP results [17] and other theoretical models [18], which were based on the experimental solution data. The latter predicted an infinite-chain limit (LO-branch of carbyne at the Γ -point) in CNTs of around $1870\text{--}1877\text{ cm}^{-1}$ [17], which is clearly above the recently observed Raman frequencies below 1800 cm^{-1} for chains in double- and multi-wall CNTs (DWCNTs, MWCNTs) [13–16]. This raises the question of how the interactions with the tube affect the Raman spectrum and its dependence on the chain length. The frequency range of near-field data gives a first hint about the effect of different tube environments for the long-chain limit. As for chains of intermediate lengths, no assignments could be made thus far and it is unclear whether chains interacting with a solvent or CNT environments feature the same convergence or saturation behavior as predicted theoretically for the bare chain in vacuo. In particular, it is not known if the typical shift between solution and CNT environment can be assumed also for longer chains and to what extent solution spectra are shifted w.r.t. to the isolated chain in vacuo. Moreover, the physics behind these environment effects remains essentially unknown.

In this letter, we report coupled-cluster CCSD(T), spin-component-scaled 2nd-order Møller-Plesset perturbation theory (SCS-MP2), and hybrid density-functional theory (DFT) calculations to demonstrate the effects of charge transfer (CT) and van-der-Waals (vdW) interactions (screening) on the vibrational properties of H-terminated polyynes encapsulated in CNTs. We find that both interactions are chain-length-dependent and will contribute a redshift that becomes more important in the limit of long chains. In consequence, the saturation of the Raman frequencies calculated in vacuo might shift towards longer chain lengths. The calculations were performed with the turbomole [22], ORCA [23], and VASP [24] software, all details are given in the Supplemental Material.

As there are no experimental IR or Raman spectra avail-

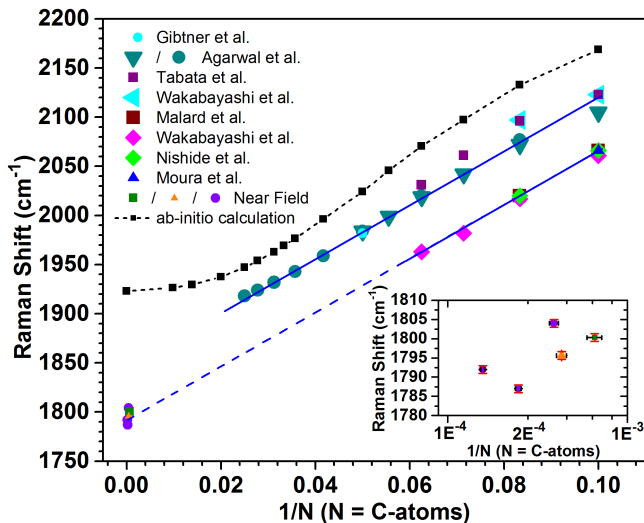


FIG. 1: Raman response of polyynes as function of inverse length given by the number N of carbon atoms. The solid lines are linear fits to the available data on chains with assigned lengths (solid symbols). The top solid line fits the data of chains in solution [6, 19–21]. The lower solid line fits data from assigned chains inside CNTs [9, 10, 12] and is extrapolated to infinite chains (dashed blue line). The inset shows the frequencies and chain lengths derived from near-field Raman microscopy images. The black dashed line with square points corresponds to theoretical SCS-MP2 results [16].

able for carbon chains in vacuo, only calculated spectra can currently serve as a point of reference for environmental effects. UV/vis spectra of short carbon chains in the gas phase [25] and in solution [21, 26–31] show that the lowest dipole-allowed optical transition is strongly redshifted in solution. For $N=16$, e.g., the shift varies from 0.47 to 0.84 eV, depending on the solvent. The redshift of short chains in CNTs is larger than any measured in solution. The λ_{\max} difference between gas-phase and solution, however, is larger than between solution and CNTs. As both the electronic transition energy (HOMO–LUMO gap) and the Raman-active Γ -mode frequency correlate with the bond-length alternation (BLA), we expect that the Raman peaks in solution reflect a significant environment shift.

In order to make a best-possible theoretical estimate for the Γ -mode frequency of polyynes in vacuo and its dispersion with chain length, we performed CCSD(T) calculations on C_NH_2 with $N=8, 10, 12, 16, 20$, and 24 (Fig. 2). Indeed, for the shortest chain, the Γ -mode frequency is 66 cm^{-1} higher than the one measured in hexane solution and the chain-length dispersion is flatter, i.e., the difference increases with chain length, reaching 107 cm^{-1} for $N=16$, or 155 cm^{-1} comparing $C_{24}H_2$ with capped chains in toluene. Longer chains were computationally not feasible at the same level of theory. Therefore, we searched for the quantum chemical method that best reproduces the CCSD(T) data without scaling the force constants. We found that spin-component-scaled variants of MP2 [32] perform significantly better than any of the tested density functionals (see Table S1 in the Supplemental Mate-

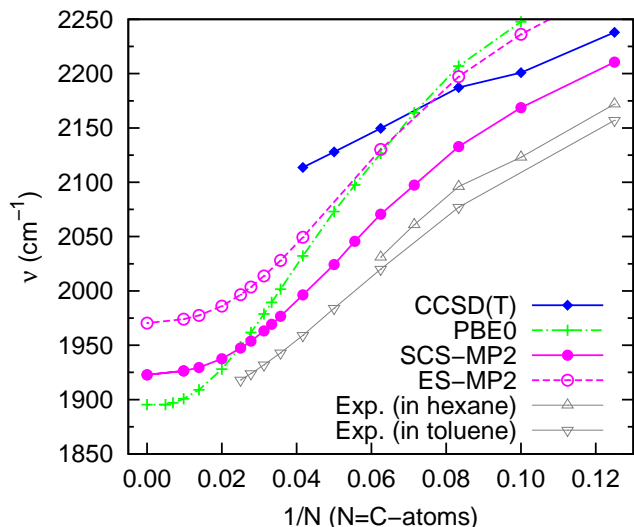


FIG. 2: Γ -mode frequency of C_NH_2 as a function of inverse chain length. Comparison of unscaled gas-phase calculations and selected experimental Raman data of H-terminated (Ref. 20) and capped chains (Ref. 6) in solution.

rial). The scaling of the two spin components in the MP2 energy expression aims at removing the systematic error in the MP2 correlation energy and is not to be confused with the empirical *a posteriori* scaling of the frequencies or force constants. The MP2 scaling parameter affects mostly the absolute frequency and not the dispersion (compare SCS-MP2 and ES-MP2 in Fig. 2). The optimal parameter, however, depends on the chain length. Therefore, the slope differs from that of CCSD(T) and rather coincides with DFT results that were scaled with the linear/exponential hybrid scheme [17]. Unscaled DFT calculations strongly overestimate the slope and the error is only partially corrected by adding HF-exchange to the functional (PBE0 data in Fig. 2, see also Ref. 33). Although sophisticated scaling schemes could be applied to also reproduce Raman frequencies of polyynes in vacuo or CNTs, the physical interactions responsible for the softening in different environments remain unknown.

Previous experiments focussed on the interaction of CNTs with very short chains ($N=8-12$) and conjectured charge transfer (CT) from the tube to the chain [11]. Theoretical works suggested inter-shell charge transfer in DWCNTs [34], which was confirmed experimentally by Kalbac et al. [35] under specific conditions. They doped DWCNTs by applying a gate voltage and analyzed the position and shape of the G band in samples that contained mostly metallic or semi-conducting outer tubes. The topology of the inner tubes was selected by the laser energy, which was matched to the S_{22} , S_{33} , or M_{11} absorption bands of the inner tubes. They found that CT requires alignment of the fermi energy with empty levels in the tubes, i.e., in case of semi-conducting tubes the gate voltage must reach the Van Hove singularities. Moura et al. [11, 12] associated changes in the shape of the G band

TABLE I: $C_{10}H_2$ in vacuo and in different CNTs.^a

	d	BLA	ν	$\Delta\nu$	Q_{chain}
vacuum		0.1040	2133	0	0.000
$C_{10}H_2@ (12,0)$	0.94	0.1038	2112	-21	-0.026
$C_{10}H_2@ (6,6)$	0.81	0.1034	2110	-23	-0.044
$C_{10}H_2@ (10,0)$	0.78	0.1035	2109	-24	-0.047
$C_{10}H_2@ (10,0)@ (18,0)$	0.78	0.1035	2108	-25	-0.056

^aPBE calculations of large supercells [6-fold for (m,0) and 9-fold for (6,6) tubes, see Supplemental Material for details]. Columns 2–6 show the tube diameter d (pm), BLA (\AA), Γ -mode frequency (cm^{-1}), shift with respect to vacuum (cm^{-1}), and net charge of the chain (e/chain atom).

with CT between short chains ($C_{10}H_2$ and $C_{12}H_2$) and SWCNTs or DWCNTs, assuming an intrinsic doping of the tubes that is reduced when the chain receives a part of the excess charge. To test this scenario, we have performed DFT calculations of short chains in different CNTs (Table I). We find only a small redshift for the Γ -mode in different tubes of 21–25 cm^{-1} . Moreover, the calculated CT from the chain to the tube is very small and minimally affects the Raman frequency. This is not surprising, as we find no indication for hybridization between the chain and tube levels and the chain LUMO is empty. We expect the applied PBE functional to overestimate CT from the tube to the chain due to the larger self-interaction error of the molecular Kohn-Sham levels. Further, the effect of CT on the frequency might be overestimated because of the above mentioned error in the phonon dispersion and slope of $\nu(N)$. Therefore, CT does not seem to fully account for the shift observed between short chains in CNTs and solution.

For long chains in double- or multi-wall CNTs, the situation is different, as the chain LUMO approaches the typical work function (WF) of these CNTs (Fig. S1). We therefore performed a DFT (PBE functional) supercell calculation of the infinite polyynene chain (HSE vacuum geometry) inside a (10,0)@(18,0) DWCNT. Fig. 3 compares the band structures of the pristine and filled DWCNT. The chain LUMO band overlaps with the valence band of the metallic outer tube, which leads to a CT to the chain of 0.022 e per chain-atom. This CT is about one order of magnitude larger than the one obtained for finite chains and comparable to calculated inter-wall CT of DWCNTs [34]. It might give rise to a measurable softening of the LO-band. The applied GGA functional, however, does not properly describe the BLA and phonon dispersion of the infinite chain. We therefore did not calculate these properties inside the DWCNT, but use the obtained CT as a parameter to estimate the effect on geometry and phonons in a smaller model system. Fig. 4 shows the results of DFT calculations using the HSE hybrid functional to optimize the infinite chain in vacuo and inside a (10,0) SWCNT when doping the system by a variable amount of excess charge. Inside the SWCNT, the excess charge localizes on the chain. Therefore, both calculations show nearly the same BLA and Γ -mode frequency for a given amount of charge. In agreement with earlier LDA calculations [36], the relation is clearly linear and the frequency shifts by 80 cm^{-1} for a CT of 0.01 e per chain

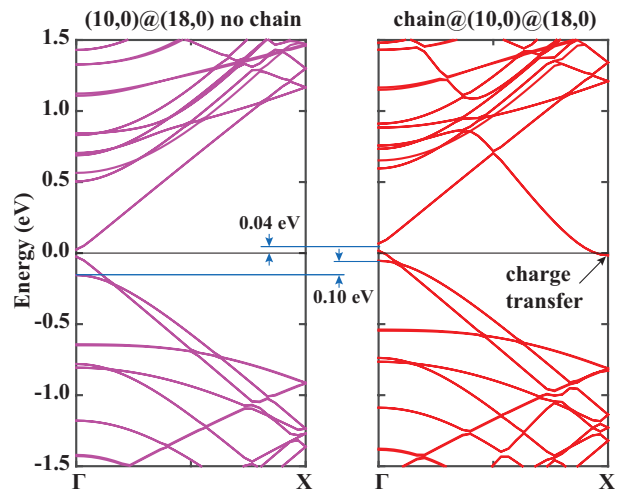


FIG. 3: Band structures of the bare (10,0)@(18,0) DWCNT (left) and encapsulating an infinite polyynene chain (right).

atom.

As the HSE functional approximates the PBE0, which overestimates the phonon dispersion (vide supra), we also performed SCS-MP2 calculations of the charged infinite chain (circular boundary condition, see Supplemental Material). We obtained a frequency shift of 61 cm^{-1} for a CT of 0.01 e per chain atom. This means that CT will cause a significant softening of the Γ -mode frequency, assuming the level alignment predicted by the GGA functional is correct. The latter should be tested at a higher level of theory, or by experiments.

VdW interactions have been associated with the redshift of the resonance energy of short chains inside SWCNTs, which increases with the tube diameter [11, 12]. These redshifts in the dipole-forbidden transitions were rather small compared to the shift of the allowed optical transition in different solvents. Moreover, the observed trend is surprising considering that the calculated interaction energy as a function of tube radius is largest in magnitude close to the vdW distance (3.3 \AA) and then decreases for larger diameters [16]. Moreover, when the tube radius is reduced in high-pressure experiments, a red shift in the Raman frequency of the chain is observed [37]. The extremely large Raman intensity of long chains in DWCNTs suggests a strong dependence of the chain polarizability on the BLA. As, on the other hand, vdW forces are approximately proportional to the polarizability α and ionization potential (IP) of the interacting species, it can be expected that the BLA is significantly affected by the tube–chain interaction, even in the absence of any CT. To test this hypothesis, we calculated the polarizability of C_NH_2 chains and its derivative with respect to displacement along the Γ -mode. They are shown in Fig. 4, together with the IP. The first two properties strongly increase with chain length, whereas the IP hardly varies. Therefore, the vdW interaction exerts a certain force on the chain that reduces the BLA and this effect increases with chain length.

The quantitative prediction of this effect is challenging, as

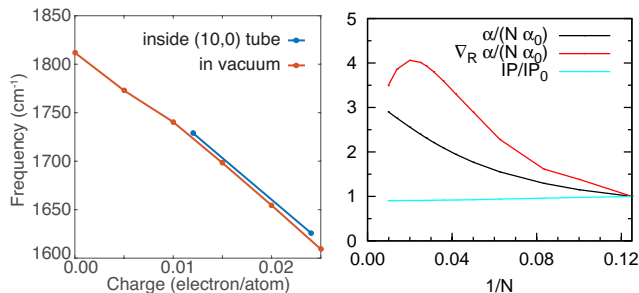


FIG. 4: Left: HSE calculation of the Γ -mode frequency of the infinite chain as a function of excess charge per chain atom. Right: Polarizability per C-atom, its derivative with respect to the displacement R along the Γ -mode, and IP. Properties are normalized with respect to C_8H_2 (α_0 and IP_0).

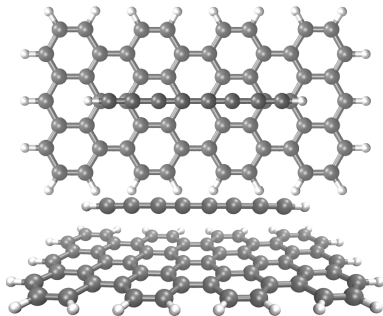


FIG. 5: Adsorption on a graphene sheet reduces the BLA of a C_8H_2 chain and softens its Raman frequency (Table S1).

the relevant electron correlation must be treated explicitly, e.g., in terms of 2nd-order perturbation theory. Pairwise vdW potentials assume fixed coefficients that do not vary with the BLA. As a simple model system, we calculated the optimized geometry and vibrational spectrum of C_8H_2 on a hydrogen-terminated graphene sheet (Fig. 5). Indeed, SCS-MP2 predicts a reduced BLA and softening of the Γ -mode frequency by 55 cm^{-1} with respect to the isolated chain (Table S1). Another ab initio method commonly used to describe vdW interactions is the random-phase approximation (RPA) [38]. It describes the same trend, but a smaller frequency shift of 14 cm^{-1} . This result might be significantly lower than the basis-set limit, as RPA is known to converge very slowly with the size of the basis set. DFT methods yield only a very small change in geometry and frequency, even when a pairwise vdW correction is applied, which produces a sheet-chain separation in good agreement with the higher-level methods. The small change in BLA and frequency is ascribed to CT from the sheet to the chain (Q_{chain} in Table S1).

We conclude that both CT and the vdW interaction soften the Γ -mode frequency of C_NH_2 chains in a tube environment, and that the effect will increase with chain length. Therefore, both have the potential to change the convergence of the Γ -mode frequency towards the infinite-chain limit. Further experimental and theoretical work is necessary to quantify the two contributions for different chain lengths. In particular CT

might be important for very long chains where the LUMO levels align with conduction band of metallic inner or outer tubes. This level alignment is difficult to predict theoretically with the required accuracy, but could be analyzed experimentally by doping a DWCNT containing a chain with a gate voltage, as accomplished for bare tubes [35]. The level alignment might also depend on the chirality and diameter of the tubes, which would be consistent with the observed structure of the chain band in DWCNTs and MWCNTs, which often features several subbands that vary with the sample [16] and with the spread of Raman frequencies in ultra-long chains, as observed in near-field Raman spectra of individual tubes [16]. The same argument applies to the vdW interaction, which might be larger in metallic than in semi-conducting inner tubes.

M.W. and A.R. acknowledge financial support by the European Research Council (ERC-2010-AdG-267374), Spanish MINECO (FIS2013-46159-C3-1-P), Grupos Consolidados (IT578-13), AFOSR Grant No. FA2386-15-1-0006 AOARD 144088, H2020-NMP-2014 project MOSTOPHOS, GA no. SEP-210187476, and COST Action MP1306 (EU-Spec). Technical and human support provided by IZO-SGI (SGIker) of UPV/EHU. S.C. acknowledges financial support from the Marie Curie Grant FP7-PEOPLE-2013-IEF project ID 628876. T.P. acknowledges support from the Austrian Science Fund (FWF, NanoBlends I 943-N19). L.S. acknowledges the scholarship supported by the China Scholarship Council. Z.J.L. and L.N. acknowledge Swiss National Science Foundation (CR2212-152944)

-
- [1] M. Liu, V. I. Artyukhov, H. Lee, F. Xu, and B. I. Yakobson, *ACS Nano* **7**, 10075 (2013).
 - [2] R. H. Baughman, *Science* **312**, 1009 (2006).
 - [3] W. A. Chalifoux and R. R. Tykwinski, *Nat. Chem.* **2**, 967 (2010).
 - [4] C. Castiglioni, J. T. L. Navarrete, G. Zerbi, and M. Gussoni, *Solid State Commun.* **65**, 625 (1988).
 - [5] B. Tian and G. Zerbi, *J. Chem. Phys.* **92**, 3892 (1990).
 - [6] N. R. Agarwal, A. Lucotti, D. Fazzi, M. Tommasini, C. Castiglioni, W. Chalifoux, and R. R. Tykwinski, *J. Raman Spectrosc.* **44**, 1398 (2013).
 - [7] X. Zhao, Y. Ando, Y. Liu, M. Jinno, and T. Suzuki, *Phys. Rev. Lett.* **90**, 187401 (2003).
 - [8] L. M. Malard, D. Nishide, L. G. Dias, R. B. Capaz, A. P. Gomes, A. Jorio, C. A. Achete, R. Saito, Y. Achiba, H. Shinohara, et al., *Phys. Rev. B* **76**, 233412 (2007).
 - [9] D. Nishide, T. Wakabayashi, T. Sugai, R. Kitaura, H. Kataura, Y. Achiba, and H. Shinohara, *J. Phys. Chem. C* **111**, 5178 (2007).
 - [10] T. Wakabayashi, T. Murakami, H. Nagayama, D. Nishide, H. Kataura, Y. Achiba, H. Tabata, S. Hayashi, and H. Shinohara, *Eur. Phys. J. D* **52**, 79 (2009).
 - [11] L. G. Moura, L. M. Malard, M. A. Carneiro, P. Venezuela, R. B. Capaz, D. Nishide, Y. Achiba, H. Shinohara, and M. A. Pimenta, *Phys. Rev. B* **80**, 161401 (2009).
 - [12] L. G. Moura, C. Fantini, A. Righi, C. Zhao, H. Shinohara, and M. A. Pimenta, *Phys. Rev. B* **83**, 245427 (2011).

TABLE II: Γ -mode frequency (cm^{-1}) and BLA (\AA) of C_8H_2 in vacuo and on top of a graphene sheet.

	ν_{vacuo}	ν_{sheet}	$\Delta\nu$	$\text{BLA}_{\text{vacuo}}$	$\text{BLA}_{\text{sheet}}$	ΔBLA	D^a	Q_{chain}
SCS-MP2	2209.9	2154.8	-55.1	0.1392	0.1298	-0.0094	3.19	-0.010
RPA	2173.6	2160.0	-13.6	0.1462	0.1442	-0.0020	3.27	
PBE0	2299.4	2298.9	-0.5	0.1343	0.1341	-0.0002	3.71	-0.003
PBE	2183.6	2182.5	-1.0	0.1100	0.1098	-0.0002	3.85	-0.003
PBE-D2	2182.3	2175.9	-6.4	0.1101	0.1094	-0.0007	3.19	-0.020
PBE-D3	2183.8	2180.1	-3.7	0.1099	0.1095	-0.0004	3.37	-0.012

^a Average separation (\AA) of the chain molecules from the surface.

- [13] A. Cupolillo, M. Castriota, E. Cazzanelli, L. Caputi, C. Giallombardo, G. Mariotto, and L. Papagno, *J. Raman Spectrosc.* **39**, 147 (2008).
- [14] M. Castriota, E. Cazzanelli, L. Caputi, A. Cupolillo, C. Giallombardo, L. Papagno, and G. Mariotto, *Diamond Relat. Mater.* **17**, 1716 (2008).
- [15] C. Zhao, R. Kitaura, H. Hara, S. Irle, and H. Shinohara, *J. Phys. Chem. C* **115**, 13166 (2011).
- [16] L. Shi, P. Rohringer, K. Suenaga, Y. Niimi, J. Kotakoski, J. C. Meyer, H. Peterlik, M. Wanko, S. Cahangirov, A. Rubio, et al., (in press, DOI: 10.1038/NMAT4617) (2016).
- [17] S. Yang, M. Kertesz, V. Zólyomi, and J. Kürti, *J. Phys. Chem. A* **111**, 2434 (2007).
- [18] A. Milani, M. Tommasini, and G. Zerbi, *J. Chem. Phys.* **128**, 064501 (2008).
- [19] T. Gibtner, F. Hampel, J. P. Gisselbrecht, and A. Hirsch, *Chem. Eur. J.* **8**, 408 (2002).
- [20] H. Tabata, M. Fujii, S. Hayashi, T. Doi, and T. Wakabayashi, *Carbon* **44**, 3168 (2006).
- [21] T. Wakabayashi, H. Tabata, T. Doi, H. Nagayama, K. Okuda, R. Umeda, I. Hisaki, M. Sonoda, Y. Tobe, T. Minematsu, et al., *Chem. Phys. Lett.* **433**, 296 (2007).
- [22] *TURBOMOLE V7.0 2015, a development of University of Karlsruhe and Forschungszentrum Karlsruhe GmbH, 1989-2007, TURBOMOLE GmbH, since 2007; available from <http://www.turbomole.com>.*
- [23] F. Neese, *WIREs Comput Mol Sci* **2**, 73 (2012).
- [24] G. Kresse and D. Joubert, *Phys. Rev. B* **59**, 1758 (1999).
- [25] T. Pino, H. Ding, F. Güthe, and J. P. Maier, *J. Chem. Phys.* **114**, 2208 (2001).
- [26] R. Eastmond, D. R. M. Walton, and T. R. Johnson, *Tetrahedron* **28**, 4601 (1972).
- [27] M. Tsuji, T. Tsuji, S. Kuboyama, S.-H. Yoon, Y. Korai, T. Tsujimoto, K. Kubo, A. Mori, and I. Mochida, *Chem. Phys. Lett.* **355**, 101 (2002).
- [28] S. Eisler, A. D. Slepko, E. Elliott, T. Luu, R. McDonald, F. A. Hegmann, and R. R. Tykwinski, *J. Am. Chem. Soc.* **127**, 2666 (2005).
- [29] G. Forte, L. D'Urso, E. Fazio, S. Patanè, F. Neri, O. Puglisi, and G. Compagnini, *Appl. Surf. Sci.* **272**, 76 (2013).
- [30] F. Cataldo, *Carbon* **42**, 129 (2004).
- [31] Y. E. Park, S. K. Shin, and S. M. Park, *Chem. Phys. Lett.* **568**, 112 (2013).
- [32] M. Gorenkamp and S. Grimme, *Chem. Phys. Lett.* **392**, 229 (2004).
- [33] M. Tommasini, D. Fazzi, A. Milani, M. Del Zoppo, C. Castiglioni, and G. Zerbi, *J. Phys. Chem. A* **111**, 11645 (2007).
- [34] V. Zólyomi, J. Koltai, Á. Ruzsnyák, J. Kürti, Á. Gali, F. Simon, H. Kuzmany, Á. Szabados, and P. R. Surján, *Phys. Rev. B* **77**, 245403 (2008).
- [35] M. Kalbac, A. A. Green, M. C. Hersam, and L. Kavan, *Chem. Eur. J.* **17**, 9806 (2011).
- [36] Á. Ruzsnyák, V. Zólyomi, J. Kürti, S. Yang, and M. Kertesz, *Phys. Rev. B* **72**, 155420 (2005).
- [37] N. Ferreira Andrade, A. L. Aguiar, Y. A. Kim, M. Endo, P. T. C. Freire, G. Bruneto, D. S. Galvao, M. S. Dresselhaus, and A. G. Souza Filho, *J. Phys. Chem. C* **119**, 10669 (2015).
- [38] H. Eshuis, J. Yarkony, and F. Furche, *J. Chem. Phys.* **132**, 234114 (2010).

Supplemental Materials: Polyne Electronic and Vibrational Properties under Environmental Interactions

COMPUTATIONAL DETAILS

Hybrid DFT (PBE0 functional [S1]) and SCS-MP2 calculations were performed with the turbomole [22] software (versions 6.1, 6.6, and 7.0). Finite C_NH_2 chains with N up to 102 were fully optimized at the SCS-MP2 level with turbomole, using a cc-pVDZ basis set. For N up to 40, the frequency of the resonant Raman active mode was calculated numerically. For $N > 40$, we used the PBE0 eigenmodes to displace the SCS-MP2 geometry and generate a harmonic fit of the potential energy surface of SCS-MP2. This approach introduces an error of less than 1 cm^{-1} (for $N > 20$) in the resulting frequency. The SCS-MP2 frequency for the infinite chain was obtained by a series of calculations of carbon rings (circular boundary condition). The ring size was increased up to 144 carbon atoms to achieve converged bond lengths and frequencies.

For the frequency calculations of the *finite* $C_{10}H_2$ chain in vacuo and inside SWCNT and DWCNT, we used the PBE and HSE functionals as implemented in the VASP 5.3.5 code [24]. For the HSE functional, a range-separation parameter HFSCREEN=0.2 was used. Like in the SCS-MP2 calculations, we employed the eigenmodes of gas-phase PBE0 calculations to obtain the force constants from the gradient of the displaced minimum-energy geometry. The following supercells and k-point samplings were used: 6-fold supercell of (10,0), (12,0), and (10,0)@(18,0) with 1 k-point and 9-fold supercell of (6,6) with 1 k-point.

For the PBE band-structure calculations of the *infinite chain* inside a (10,0)@(18,0) DWCNT, we used a 3-fold supercell of the DWCNT, which hosts 10 chain atoms. We used the equilibrium bond lengths of the chain in vacuo as obtained with the HSE functional. We did not optimize the chain inside the tube, because the GGA functional does not properly describe the BLA and favours a cumulenic structure inside CNTs [36]. The box size was adjusted to the chain geometry. 31 irreducible k-points were used.

For the C_8H_2 @graphene calculations, a saturated graphene sheet of 78 atoms was used (Fig. 5 in the main article). The geometry was fully relaxed with turbomole using SCS-MP2 (cc-pVDZ basis set), or DFT [SV(P) basis set]. The eigenmodes from gas-phase PBE0 calculations were employed to obtain the force constant of the Γ -mode. For C_8H_2 in vacuo, the resulting errors were smaller than 1 cm^{-1} when compared with the frequency from the full analytical Hessian.

CCSD(T)/cc-pVDZ geometry optimizations were performed with turbomole version 7.0.2 using symmetry-adapted numerical gradients. CCSD(T) frequencies were obtained using the displacements of the SCS-MP2 eigenmodes or (for $N=20, 24$) those of the PBE0 Hessian (see above).

Benchmark calculations (see below) for the geometry of $C_{12}H_2$ were performed with ORCA using the cc-pVDZ basis set.

[S1] J. P. Perdew, M. Emzerhof, and K. Burke, J. Chem. Phys. **105**, 9982 (1996).

TABLE S1: $C_{12}H_2$ RMSD of the energy gradient (atomic units) of the CCSD(T) geometry.

Method	RMSD
CCSD(T)	0.0000
ES-MP2 ^a	0.0028
ES-MP2 ^b	0.0033
SCS-MP2	0.0042
SCS(MI)-MP2	0.0045
B2GP-PLYP	0.0052
mPW2PLYP	0.0053
B3LYP	0.0065
M06	0.0067
PBE0	0.0068
B2PLYP	0.0071
PBE28	0.0072
PBE20	0.0073
BMK	0.0076
PBE30	0.0077
TPSS0	0.0078
HISS	0.0119
MP2	0.0136
wB97XD	0.0143
M062X	0.0146
tHCTh	0.0146
CAM-B3LYP	0.0150
PBE	0.0173
M11	0.0192
LC-PBE	0.0293
HF	0.0431

^aMP2 with equally-scaled spin components (ES-MP2), optimized scaling parameter of 0.763.

^bES-MP2 with scaling parameter of 0.73.

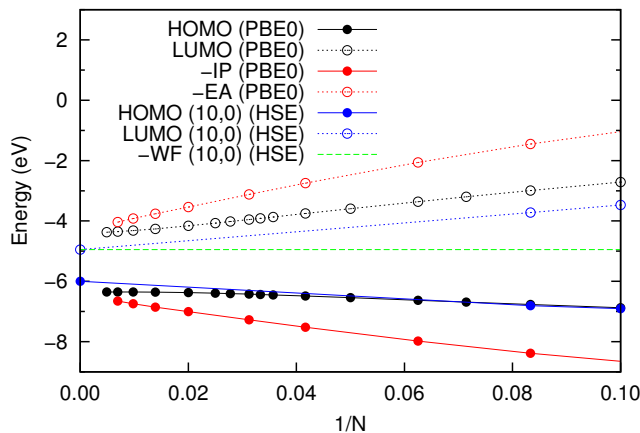


FIG. S1: Comparison of electronic levels, EA, and IP of $C_N H_2$ in vacuo and inside SWCNT (HSE calculation) and the work function of a (10,0) SWCNT (HSE calculation).